PAPER

Impact of divertor configuration on recycling neutral fluxes for ITER-like wall in JET H-mode plasmas

IOP Publishing Plasma Physics and Controlled Fusion
Plasma Phys. Control. Fusion **62** (2020) 035006 (15pp) https://doi.org/10.1088/1361-6587/ab5fb1

Impact of divertor configuration on recycling neutral fluxes for ITER-like wall in JET H-mode plasmas

E de la Cal[1], U Losada[1], A Martín de Aguilera[1], A Shaw[2], E Solano[1], D Alegre[1,3], I Balboa[2], P Carvalho[2], J Gaspar[4], I Borodkina[5], S Brezinsek[5], D Douai[6], C Giroud[2], C Guillemaut[2], C Hidalgo[1], A Huber[2], E Joffrin[6], T Loarer[6], E de la Luna[1], A Manzanares[1], F Militello[2], L de Pablos[1], S Wiesen[5] and JET contributors[7]

[1] Laboratorio Nacional de Fusión, CIEMAT, Av. Complutense 40, E-28040 Madrid, Spain
[2] CCFE Fusion Assoc., Culham Science Centre, Abingdon, OX14 3DB, United Kingdom
[3] Departamento de Ingeniería Energética, UNED, C/Juan del Rosal 12, E-28040 Madrid, Spain
[4] Aix Marseille Univ, CNRS, IUSTI, Marseille, France
[5] Forschungszentrum Jülich GmbH, Institut für Energie-und Klimaforschung—Plasmaphysik, D-52425, Jülich, Germany
[6] CEA, IRFM, F-13108 Saint-Paul-lez-Durance, France

E-mail: e.delacal@ciemat.es

Received 3 April 2019, revised 4 December 2019
Accepted for publication 6 December 2019
Published 16 January 2020

Abstract

In recent years it has been well known that in JET, with the ITER-like wall, the performance of high-power H-mode plasmas depends strongly on the magnetic topology of the divertor. This is generally attributed to the effect of the magnetic field shaping on the neutral flux transport and pumping, which —in high density H-mode plasmas—determine the pedestal properties and the global confinement. In this work we have analysed the spatial distribution and the dynamic behaviour of the D_α-emission for different magnetic configurations. Experimental observations indicate that for certain configurations, the surface temperature and the D_α—emission anomalously increase on top of the inner divertor, which points to thermal outgassing there. This is also the region where most beryllium co-deposits accumulate and most deuterium becomes trapped. The overheating at this region far from the strike point (SP) is observed to happen in magnetic configurations with reduced distance between the divertor material surface and the separatrix (clearance). The neutral flux that appears at the upper inner divertor during a few milliseconds after the ELM-crash, is more than an order of magnitude larger than the gas puffing rate and dominates over all other regions. Finally, a preliminary study describes how this thermal fuel outgassing from the co-deposited layers could be used intentionally as a wall-conditioning in JET technique with plasmas that focus their particle and heat flux there. This could be used as a complementary wall isotope control technique and more specifically for tritium recovery from the upper inner divertor where most fuel-trapping beryllium co-deposits accumulate in JET ITER-like wall.

Supplementary material for this article is available online

Keywords: plasma-wall, recycling, fuel inventory, outgassing, magnetic configuration

(Some figures may appear in colour only in the online journal)

[7] See X Litaudon *et al* 2017 (10.1088/1741-4326/aa5e28) for the JET contributors.

1. Introduction

Since the installation of the ITER-like wall (ILW), JET has demonstrated successfully the compatibility of an all-metal wall with reactor relevant high power H-mode scenarios. The benefit is reduced fuel trapping in the vacuum vessel by at least one order of magnitude with respect to the carbon divertor [1–4]. The latter exhibited a prohibitively large wall fuel accumulation due to the strong chemical reactivity of carbon with hydrogen isotopes. The hydrocarbons generated by the plasma were demonstrated to have a high sticking capacity at remote and hidden surfaces producing thick hydrogenated carbon co-deposits. No reliable cleaning method to remove these deposits was found. The reactor vessel tritium (T) inventory predicted due to this effect showed that it would have been impossible to maintain operation within safety limits for a reasonable fusion plasma burn time; only a few hundred 6–7 min ITER plasmas would have been sufficient to exceed this limit. With such pessimistic predictions, the use of carbon (C) as the primary plasma facing component (PFC) for next step burning reactors had to be abandoned and metallic PFCs appeared as the alternative. The promising JET-ILW results allowed the fusion community to gain confidence in reactor relevant plasma scenarios with an all-metal environment and ITER will operate from the beginning with a beryllium (Be)—tungsten (W) first wall. The planned preliminary operation phase with a carbon divertor has been removed from the plan, thereby reducing both costs and the time until D (deuterium)-T operation.

Moreover, during this last JET period, valuable experience has been gained in plasma operation with an all-metal wall, which has been shown to have behaviour not seen before with the C divertor. New 'hidden parameters' appear that are being studied in order to understand the physics of H-mode plasmas see e.g. [3, 4]. For example, during the first years of JET-ILW operation, H-mode confinement was reduced by at least 20% in the so-called ITER Baseline scenario (normalised pressure ratio $\beta_N \approx 1.5$) with respect to the carbon wall. Good confinement was demonstrated to be partially recovered with nitrogen seeding [5]. This degradation in confinement was attributed to the large fuel puffing necessary to reduce the plasma edge temperature at the divertor targets in order to minimise W sputtering and its subsequent accumulation in the plasma centre. This is believed to be the origin of the temperature decrease in the pedestal and core plasma, leading to the performance degradation. More recently it was discovered that global confinement could be improved for specific magnetic configurations, with the best performance (confinement factor $H_{98Y} \approx 1$) obtained with the SPs located at the divertor corners near the pumping conduits (here called Corner- or C-configuration), where recycled neutral exhaust is most efficient [6–11], see figure 1.

This observation addresses once again the effect of the neutral density (or pressure) on the scrape-off-layer (SOL) plasma. Generally speaking, high neutral densities degrade the pedestal properties and finally the global plasma confinement. Unfortunately, to date there is no clear understanding of the physics behind it. Simulations show that energy losses of neutrals entering the confined region are minimised with the SP near the pumping openings at the divertor corners, but the quantitative values are far from the observed differences in confinement [9]. On the other hand, the increase of the main chamber neutral pressure has been linked with the outer SP distance from the divertor pumping openings at the corner, which negatively affects plasma pedestal pressure [11]. This empirical observation was noted many years ago and the energy confinement time was observed to scale directly with neutral pressure in the main chamber see e.g. [12, 13]. In JFT-2M tokamak was found that a sufficiently strong local gas-puff may cool down the edge T_e thereby reducing the neutral ionisation rate and the fuelling efficiency. A critical neutral pressure at the outer mid plane for the onset of this effect of about 10^{-3} Pa was measured. The increased edge neutral and plasma density raises the radiation and charge—exchange losses inducing the confinement degradation. The use of a pumped limiter reduced this effect sensibly [14, 15]. A more recent explanation of the confinement degradation with the neutral density increase is discussed in [11]. It links the main chamber neutrals with the radial electric field change, which enhances the rotational shear at the plasma edge, reducing perpendicular transport. For further information concerning the effect of divertor geometry and magnetic configuration on many different parameters such as the pumping efficiency, target power loads, ionisation sources and detachment, etc, the reader is referred to [16]. For modelling aspects of neutrals including

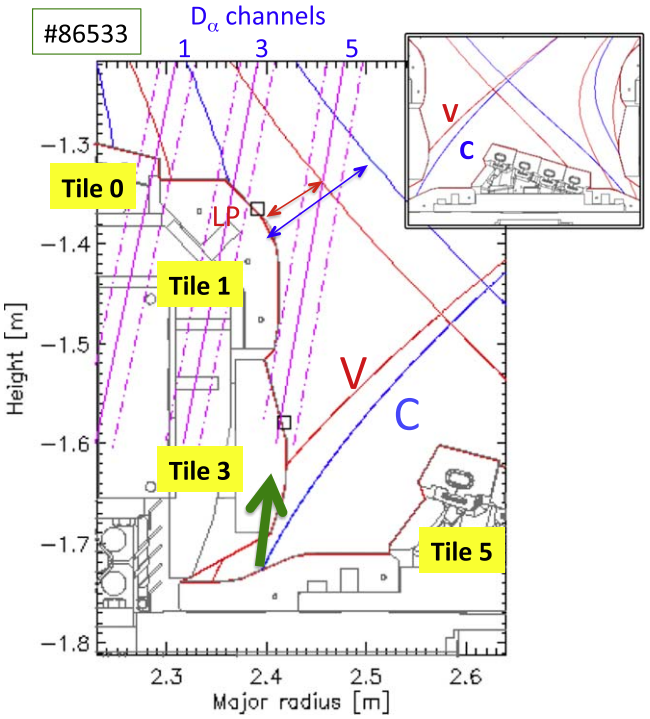

Figure 1. Divertor magnetic configurations of plasma #86533 showing the Corner (C) and Vertical (V) configurations. Also shown are some inner D_α-channels and the uppermost Langmuir probes (LP).

molecular dynamics in ITER and its influence on divertor performance the reader is referred to [17] and references therein.

Since operation with the ILW, the physics of recycling has varied considerably. This was to be expected due to the very different characteristics of C and W when exposed to D fluxes [1, 18–25]. For example W has a much larger reflection coefficient compared to C, and a much lower capacity to adsorb D, except in regions where Be co-deposits grow. Moreover, recycling, which is the re-emission by the plasma-facing material of D as a response to the ion and heat fluxes, should be seen as a dynamic process if transient events such as ELMs are present. Therefore, the physics of ELMy scenarios in the SOL and edge plasma is a complex kinetic plasma-wall interaction process where the neutral, ion and heat transport must be balanced. Some aspects of the recycling and pedestal recovery dynamics in JET with the new ILW have been described recently see e.g. [21–25]. More generic modelling of the dynamics of the surface response during ELMs can be found in [26, 27]. There is also an experimental study on the recycling coefficient's fast variations during ELM-like events in the TJ-II stellarator [28]. Finally, a theoretical study of the fuel absorption and re-emission kinetics has been done for W when exposed to ELMs using a diffusion-trapping model, simulating quantitatively the incident power and particle fluxes [29].

In the present work we study the spatial distribution and dynamic behaviour during ELMs of the recycling neutral fluxes at the divertor for high-power H-mode plasmas with different magnetic configurations. The total heating power $P > 15$ MW was mainly through neutral beam injection (NBI), occasionally with a small fraction of ion cyclotron range of frequencies (ICRF) heating. More specifically the effect of the proximity of the SPs to the divertor corners near the pumping conduits is compared for similar plasmas, as done in previous studies [6–11]. The main analysis has been done comparing the spatial distribution of the D_α-emission and its dynamics during ELMs at the inner divertor, since the neutral fluxes dominate there for the studied plasmas.

In previous work it has already been observed [24], that for certain magnetic topologies, the D neutral fluxes strongly increase for high power H-mode plasmas on top of the inner divertor just after the ELM-crash. This was initially surprising because this region is relatively far from the SP position. The D emission came from the region where surface analysis has shown that most D becomes trapped within the Be co-deposits that preferentially accumulate there. Therefore we proposed already in [24] that local fuel outgassing due to surface over-heating could be the reason for the increased neutral flux. Also in a recent study, during the change-over from a deuterium to a hydrogen campaign, a strong spatial inhomogeneity of the plasma isotope ratio in the divertor was observed [30]. This phenomenon was attributed to local re-emission of the fuel isotope of the previous campaign that was trapped in the Be co-deposits of the inner divertor.

The goal of the present work is to try to understand this outgassing phenomenon in more detail. Therefore, we analyse the surface temperature evolution using thermography to show that there is a clear correlation with the D_α-emission increase at this divertor region. The neutral flux generated during a few milliseconds after the ELM-crash is estimated using the absolutely calibrated D_α-radiance. It is more than an order of magnitude larger than the puffing rate and dominates the recycling neutral fluxes in the divertor. Different examples indicate that the anomalous overheating of the upper inner divertor tiles that induce the D outgassing is linked to the magnetic configuration and, more specifically, to the distance of the plasma separatrix from the material surfaces in this region.

In a final section we show how this local outgassing from the upper inner divertor region induced by the plasma heating could be used to intentionally desorb the fuel accumulated there. This could be useful for wall isotope control and fuel inventory reduction in future JET campaigns with T [31].

2. Experimental

The discharges analysed here are high-power ($P \geqslant 15$ MW) H-mode plasmas with plasma current $I_P \geqslant 1.8$ MA and a toroidal magnetic field $B_T \geqslant 2$ T. We always compare pairs of plasmas with similar heating power, triangularity and gas injection rate but with different divertor magnetic configurations. More specifically, we compare the effect of the proximity of the SPs at the divertor corners near the pumping conduits for similar plasmas as in [6–11].

We analyse the visible plasma emission, mainly the D_α-atomic line, to get information about the neutral fluxes. The main diagnostic used is a D_α-spectroscopy system with narrow band-pass filters that views the divertor in 20 chords from an upper vertical port on the machine. The radiance is absolutely calibrated and has an acquisition frequency of 100 kHz. Also, two spectrometers were used two analyse the D_γ/D_α ratio. Additionally, we also analyse the visible emission with a Fast camera with up to 70 kHz sampling rate [32] and a slow (30 Hz) intensified D_α- and D_γ-filtered camera. Both have a tangential view of the divertor [33].

To measure the divertor surface temperature the thermal radiation is analysed with a mid wave infrared (MWIR) camera and a near infrared range (NIR) filtered visible camera. The MWIR camera [34, 35] works in the 3–5 μm range and has a sampling rate of about 15 Hz. The exposure times for the plasmas analysed here is in the range of 0.5 milliseconds. The NIR camera is part of the JET Protection System [36, 37]. The camera filters light from the NIR range to extract from the thermal (blackbody) radiation the surface temperature. The filter is centred at $\lambda = 1016$ nm and has a bandwidth of ± 40 nm. It is absolutely calibrated for $T > 800$ °C and its recording speed is 50 Hz. Unfortunately, other plasma emission sources can contaminate the thermal radiation from volume plasma emission such as Bremsstrahlung and free-bound transitions from recombining processes [37]. It should be clarified that the surface emissivity is a free parameter when obtaining the absolute temperature from the thermal emission and depends on the surface properties. Since plasma exposed surfaces can continuously vary their

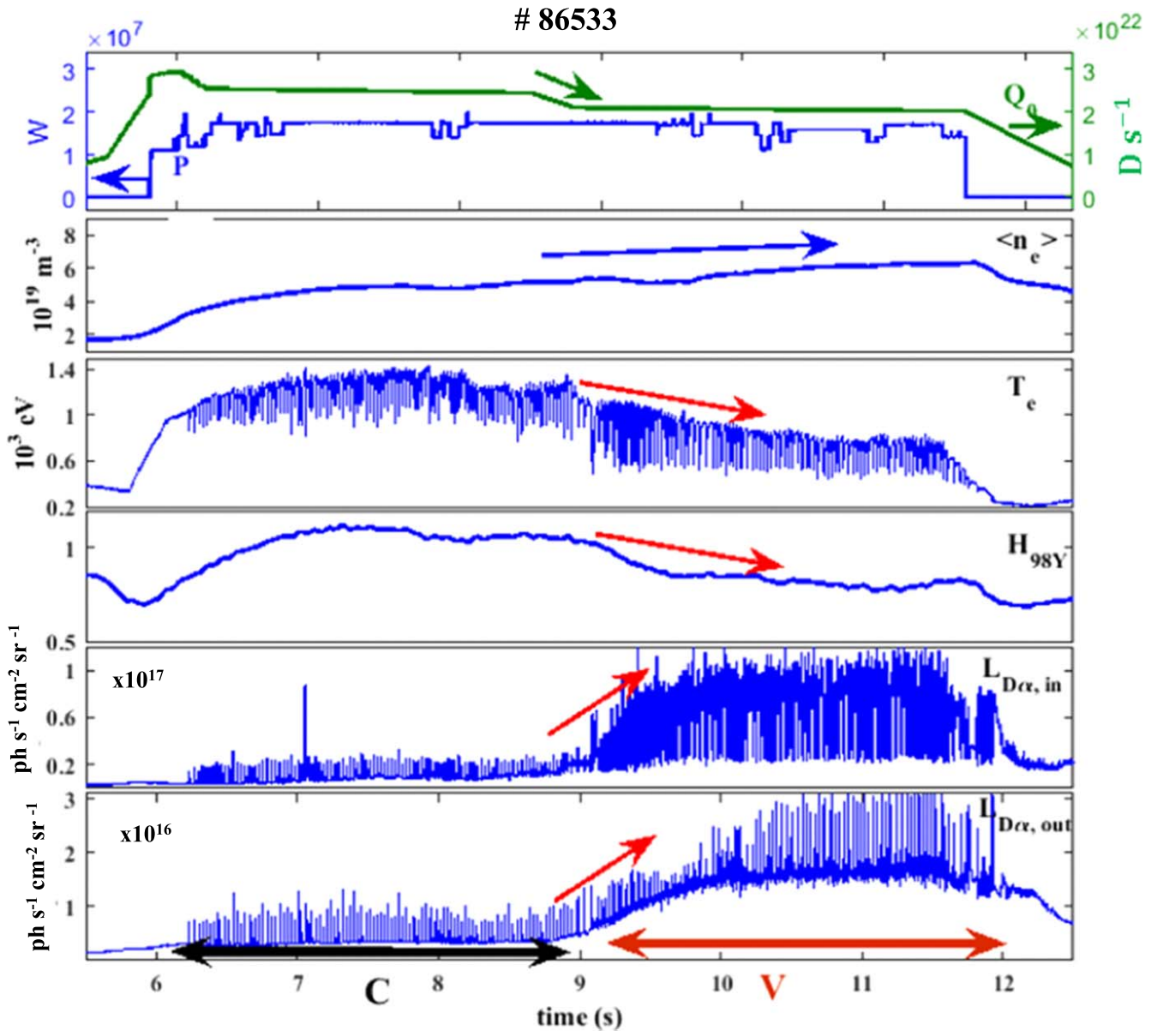

Figure 2. Time traces of the NBI power P, puffing rate Q_0, plasma average density $\langle n_e \rangle$, pedestal electron temperature T_e, the H_{98Y} confinement factor and the integrated inner and outer divertor D_α-emission radiance $L_{D\alpha}$. The arrows at the horizontal axis mark the C- and V-configuration phases.

emissivity, an uncertainty in the measurement must be kept in mind. Here an emissivity of 0.18–0.24 (depending on the temperature range) for the upper inner W-coated carbon divertor tiles was selected. The software framework JUVIL [38] was used to analyse thermal and visible camera videos are available online at stacks.iop.org/PPCF/62/035006/mmedia.

3. Experimental observations at the inner divertor: 'Corner' versus 'Vertical' configuration

3.1. Global plasma modifications

Figure 1 shows the two divertor magnetic configurations used in discharge #86533. This plasma had the following parameters: $B_T = 2.4$ T, $I_P = 2.5$ MA, $P = 17$ MW (NBI) + 1.5 MW (ICRH) and has already been analysed in previous work [6]. During the H-mode, the plasma begins with the inner SP near the divertor pumping openings (here called Corner or C-configuration) and is moved after 2 s to the vertical target (here called Vertical- or V-configuration). Also shown are some inner D_α-chords (channels 1, 3 and 5) and the uppermost Langmuir probe (LP). Figure 2 shows several time traces where the strong influence of the divertor magnetic configuration on the plasma parameters can be seen. Plotted are the signals during the H-mode phase of the NBI power, the plasma average density $\langle n_e \rangle$, the pedestal electron temperature T_e, the H_{98Y} confinement factor and the integrated inner and outer divertor D_α-emission radiance $L_{D\alpha}$. The magnetic topology passes from C- (black arrow) to V-configuration (red arrow) at $t = 9$–10 s. The D puffing rate

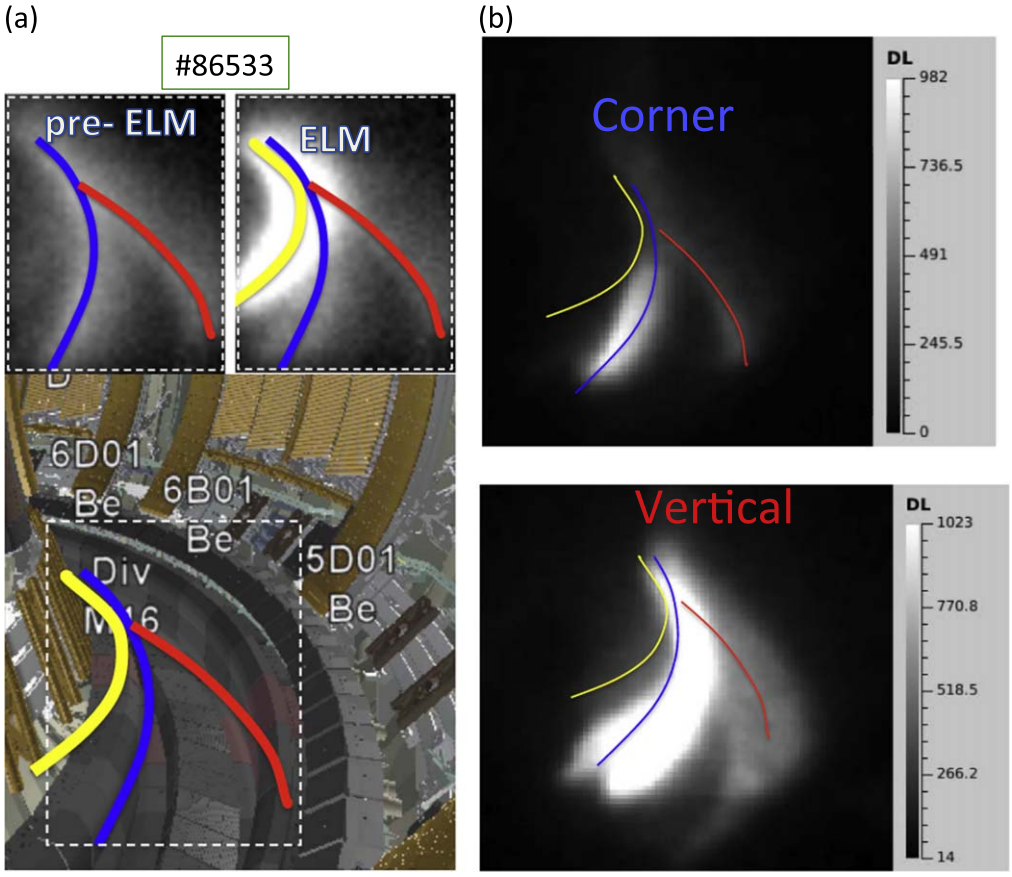

Figure 3. (a) Two frames of the divertor taken with the visible Fast camera during the V-configuration of #86533: left before the ELM, right after the ELM, and below the CAD view of the camera to the divertor (see text). (b) Corresponding images from video-clips of the Corner- (up) and the Vertical-configuration (down), (available online at stacks.iop.org/PPCF/62/035006/mmedia). The grey scale represents the camera digital level (DL) in arbitrary units and is a measure of the plasma visible emission intensity.

Q_0 was firstly set to 2.5 × 10^{22} D s^{-1} and was reduced to 2 × 10^{22} D s^{-1} during the V-configuration (it is schematically shown at the upper frame in blue). Note that even with the puffing reduction, $\langle n_e \rangle$ increases. The degradation of the confinement when going to V-configuration is clear: T_e drops significantly and the confinement factor H_{98Y} decreases from 1.05 to 0.85. The central T_e falls from about 6 to 4 keV (not shown). The divertor plasma also shows considerable changes. During the C-configuration, the global inter-ELM D_α-fluxes are a factor of 3 larger at the inner divertor than at the outer. When going to the V-configuration they increase by a factor of 3 at the outer and by a factor of 10 at the inner divertor, indicating an enhanced neutral D flux there. The D_α-emission dynamics during the ELMs and its spatial distribution changes will be shown in more detail in the next section. These general trends of the plasma parameters when changing the divertor configuration from Corner- to Vertical- also occur in the plasmas shown in the past [6–11].

3.2. D_α-emission response to divertor magnetic topology changes

Figure 3(a) shows two frames of the divertor taken with the visible Fast camera during the V-configuration of the same plasma #86533: left, before the ELM and right, after the ELM. Below shows the CAD-view of the camera into the divertor. The coloured lines indicate schematically the different emission regions: in red the outer SP-line, in blue the inner one and in yellow the upper inner divertor region. Note that a strong emission-cloud appears at the high-field side (HFS) just after the ELM. The accurate location of these emission regions were performed by applying the 'cross-correlation technique' between different region of interest (ROI) of the camera data and the spatially-well defined D_α-chord radiances looking from the upper port to the divertor. The camera had no filter for this discharge but the dominant emission by far at the divertor is D_α-atomic line emission. A proof of this is the high cross-correlation yield with the D_α-spectroscopy channels once the correct lines were obtained. Also, videos of similar discharges with and without D_α-filter are nearly equal, except with a higher intensity level without the filter (because of the transmission losses). The camera was operated with 10 μs exposure time and 25 kHz recording speed.

Figure 3(b) shows images from two video-clips that are available online at stacks.iop.org/PPCF/62/035006/mmedia, at the top the one of the Corner- and below of the Vertical-configuration. The grey scale represents the camera digital level (DL) in arbitrary units and is a measure of the plasma visible emission intensity. The clips show two ELM cycles,

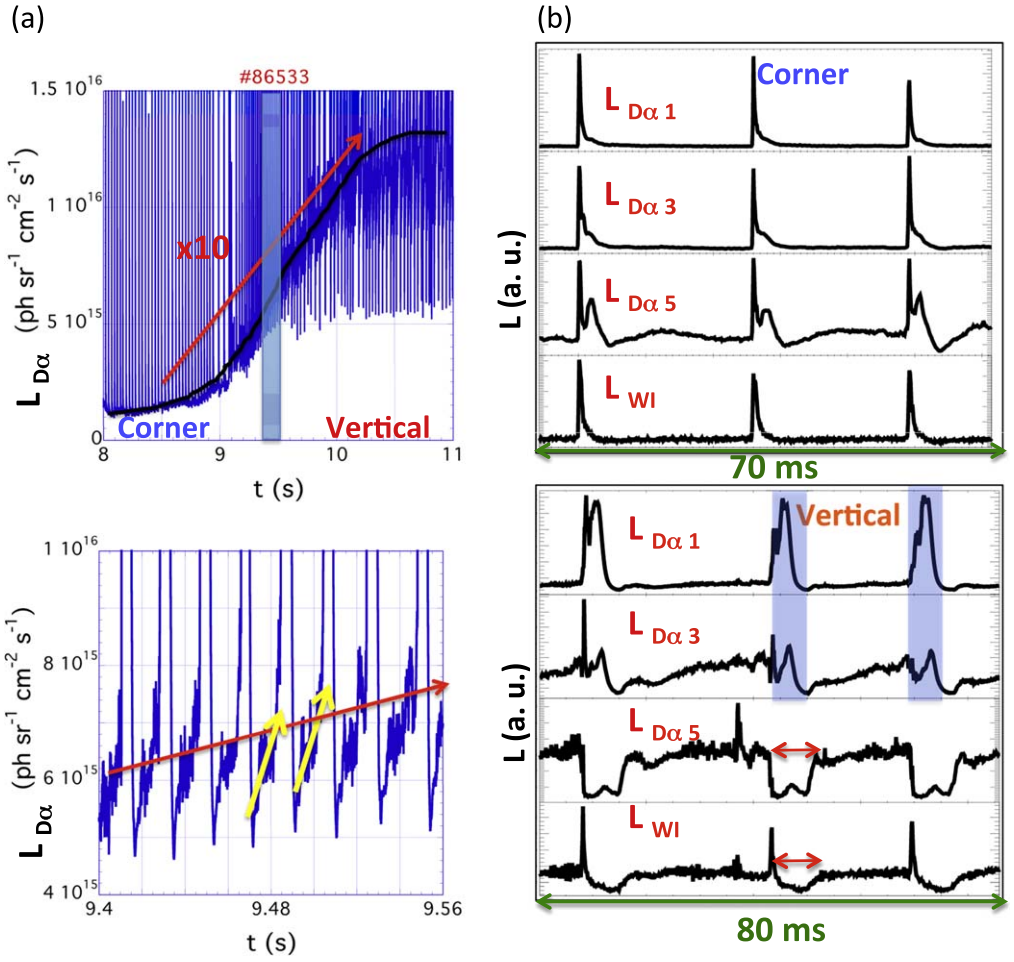

Figure 4. (a) Inter-ELM level evolution of the innermost D_α-channel radiance $L_{D\alpha}$ looking to the corner between tiles 0 and 1. (b) Time traces of D_α- radiance of channels 1, 3 and 5 (see figure 1) and total inner divertor WI radiance during C- (up) and V-configuration (down).

corresponding to about 50 ms of plasma time. One of the clips corresponds to a very similar discharge with the same parameters and configuration change as #86533. This is because for this high framing speed the camera buffer memory limits the video recording time to about two seconds and therefore two consecutive 'twin-discharges' were necessary to record the full H-mode period. The movement of the image is due to the ELMs, which produce vibrations in the camera supporting structure that is fastened to the tokamak vessel. Looking to the videos, we see that in the C-configuration, the ELMs are faster and the inter-ELM equilibrium pattern is recovered rapidly. In contrast, in the V-configuration, a strong emission cloud appears at the HFS just after the ELM-crash that dominates intensity in the whole divertor. This cloud is located at the upper inner divertor region on top of tiles 0 and 1 as shown in figure 3(a).

Figure 4(a), upper frame, shows for the same discharge the inter-ELM D_α-radiance $L_{D\alpha}$ during the configuration change as obtained from the innermost spectroscopy channel that looks to the corner between tiles 0 and 1 (see figure 1). The intensity increases during the configuration change by a factor of ten. Below is a zoom of the blue frame of the upper figure. It can be seen that in-between ELMs the D_α-emission continuously increases (yellow arrows), which makes the inter-ELM intensity monotonically increase during the configuration change (red arrow).

The ELM D_α-emission dynamics during the stationary phases of the C- ($t < 9$ s) and V-configuration ($t > 10$ s) is shown in figure 4(b) for channel numbers 1, 3 and 5 (see figure 1). Below the total inner divertor WI radiance is also shown to visualise the ELM-crashes. The ELM frequency is about 40 Hz in both phases. In the C-configuration, all D_α-channels have positive peaks during the ELM-crash. Also a secondary peak appears for the views that look directly at the SP. In the V-configuration the emission dynamics completely change. The innermost two channels that look at the inner upper horizontal divertor (tiles 0 and 1) show strong emission peaks that last about 5 ms longer than the ELM-crash. These correspond to the post-ELM emission cloud seen with the fast camera. Channel number 3, which looks at the inner divertor corner, sometimes shows no clear spike at the ELM-crash, but the secondary peak as in channel numbers 1 and 2 is present. The emission of channel number 5, that looks at the inner SP (channel number 5), decreases just at the ELM-crash during about 8 ms (red arrow). These so-called 'negative ELMs' are characteristic of a (partly-) recombining, cool and high-density SOL plasma that develops near the SP. Note also that during these periods the WI flux decreases,

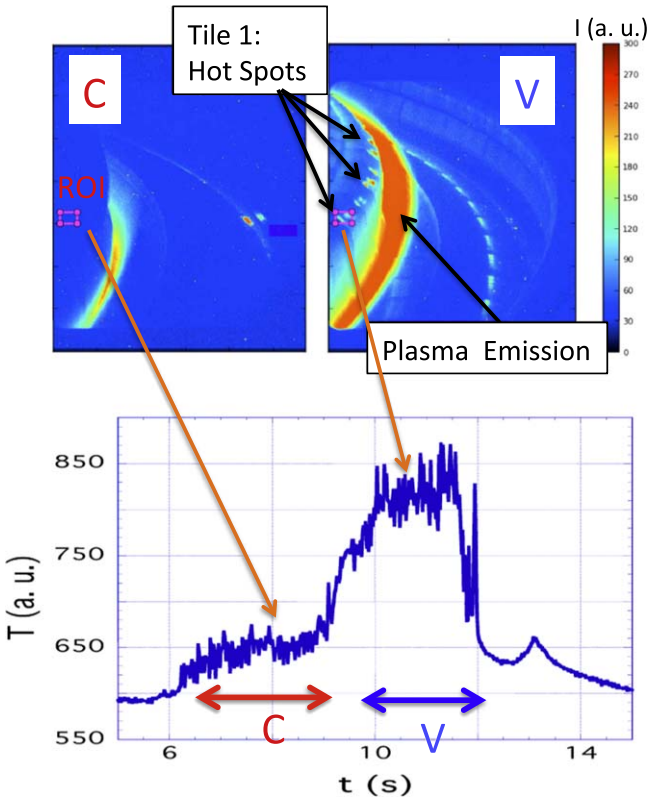

Figure 5. The upper pictures show two frames of the NIR camera video (in false colour scale), left in C-, right in V-configuration, and the lower part shows the time evolution of the average intensity of the selected ROI at tile 1. The corresponding video clip can be downloaded from stacks.iop.org/PPCF/62/035006/mmedia.

probably due to the reduced T_e that lowers the sputtering at the targets.

When comparing quantitatively all divertor D_α-channels, including the outer ones, we observe that in the approximately 5 ms post-ELM period, the contribution from the innermost 3 channels is dominant in the V-configuration. Since the D_α-radiance $L_{D\alpha}$ is absolutely calibrated, the post-ELM neutral D flux F_0 at the upper inner divertor region can be estimated assuming ionising conditions there:

$$F_0 = 4\pi\, A(S/XB)L_{D\alpha}, \qquad (1)$$

where the observing area A corresponds to the projection of the divertor disc of about 12 cm radial extension that is observed by the three innermost chords and the number of ionisation events per photon $S/XB \approx 20$ (see e.g. [25]). We can assume ionising conditions since recombination does not contribute at least significantly to the neutral fluxes in this region as is shown in the separate appendix. From equation (1) we obtain a D neutral flux of about $F_0 \approx 5 \times 10^{23}$ D s^{-1} during the post-ELM peak coming from the horizontal upper divertor region covered by the first three D_α-chords. This is a significant quantity, a factor of 25 higher than the puffing rate ($\approx 2 \times 10^{22}$ D s^{-1}).

3.3. Correlation of thermal radiation to post-ELM D_α-emission

The post-ELM neutral fluxes from the upper inner divertor region described in the paragraph above were observed systematically for a large number of high power H-mode plasmas (see later for further examples). As already disclosed in a previous work [24], the origin could be local thermal desorption due to the power deposited by the ELMs. In fact, the observed D_α-emission location on top of tiles 0 and 1 coincides with the region where most D containing beryllium co-deposits accumulate, as deduced from surface analysis studies [39, 40]. If this is true, in order to generate the outgassing of trapped D, an increased power load must occur that overheats the surfaces at this region, which should be correlated with the observed local increased D_α-emission. Moreover, if this correlation is found, it would be interesting to understand the cause of this local overheating, most probably linked to the magnetic divertor configuration. These points will be analysed first in this section for the plasma described above and in the next section other examples will be studied.

For the discharge #86533 analysed above, unfortunately the MWIR thermography camera looking at the inner divertor was not operative. We therefore studied the data from a NIR Protection Camera that looks tangentially with a similar view to the visible Fast camera. As disclosed in section 2, these kinds of cameras are only calibrated for very high temperatures $T >$ 800 °C. Additionally, in many situations, other emission sources contaminate the thermal radiation filtered at this range, such as plasma Bremsstrahlung and emission due to atomic free-bound transitions from recombining processes. This contamination can be dominant especially in cool high-density plasma conditions as will be shown. The top section of figure 5 shows two frames of the video of this NIR camera in a false colour scale during the

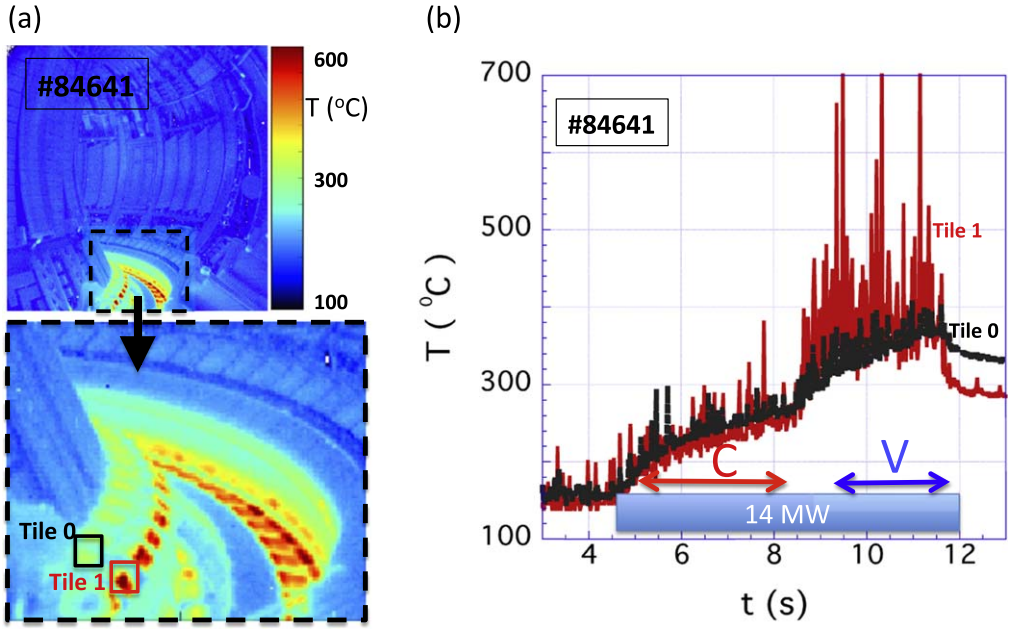

Figure 6. (a) Wide-angle view of the MWIR camera for plasma #84641 and below a zoom of the divertor where two ROIs at tiles 0 and 1 are shown. (b) Time evolution of the maximum temperature of the selected ROIs during the H-mode, the arrows indicating the C- and V-configuration phases.

H-mode phase of plasma #86533. The video-clip can be downloaded from stacks.iop.org/PPCF/62/035006/mmedia. The transition from the C- to the V-configuration takes place at about $t = 12$ s of the clip. The change in the emission pattern is clear. During the C-configuration, light at the inner divertor only comes from a narrow region corresponding to the SP line. When passing to the V-configuration, this emission cloud expands and becomes stronger, while a brilliant emission regions appear on top of tile 1. The origin of the toroidal emission cloud is volume plasma emission characteristic of a dense and cool plasma, but the light from the bright discrete areas with sharp contours at tile 1 is mainly surface thermal emission indicating local overheating (hot spots). An ROI has been selected on top of tile 1 around one of these hot spots and the time evolution of the average intensity in this ROI is represented in the lower figure. The time trace shows a clear increase when the configuration changes from corner to vertical indicating a local temperature raise.

Since, due to the light contamination, a quantitative estimation of the surface temperature is not possible for this plasma with the NIR Protection camera, another similar plasma of the same experiment was selected for which data of the MWIR thermography camera were available. Discharge #84641 has a very similar divertor configuration change during the H-mode as the one analysed before (#86533), although with 3 MW less NBI power, no ICRF power and also somewhat lower B_T and I_P. Figure 6(a) shows a frame of the MWIR camera for this discharge and below is a zoom of the divertor. Two ROIs were selected at tiles 0 and 1. The time evolution of the maximum temperature of both ROIs is shown in figure 6(b) during the H-mode, the arrows indicating the C- and V-configuration phases. A clear raise of the base-temperature, from about 200 °C–250 °C to 300 °C–400 °C is visible at tiles 0 and 1 when the configuration changes to V. Additionally, strong temperature spikes appear at tile 1 reaching values >700 °C. Only a few ELM-crashes (duration time is ≈ 1 ms) are randomly captured by the camera because of its long 'dead time' without data. In other words: since the time between two consecutive frames is 65 ms but the sensor exposure time just 0.6 ms, only a fraction of ELM-crash events, which appear approximately every 25 ms, are captured. It should be noted that higher temperatures are to be expected for the discharge analysed before (#86533), since the heating power was higher.

On the other hand, laboratory measurements by thermal desorption spectroscopy have shown that the outgassing of D trapped in Be co-deposits happen at discrete characteristic temperatures, which begin with a strong desorption peak at about 300 °C–350 °C [41, 42]. These values seam to be reached and even well surpassed during ELMs at tiles 0 and 1 during the V-configuration phase. We can therefore say that, at least potentially, during this plasma phase D may be desorbed from the co-deposits. It should be remembered, however, that due to the possible error in the temperature estimation (see section 2), this quantitative measurements should be confirmed in future studies as discussed later.

Once it is confirmed that for certain high-power H-mode plasmas the threshold temperature for D outgassing is very probably reached and surpassed at tiles 0 and 1, it would be interesting to understand the origin of this anomalous overheating. Initially, when looking into the magnetic configuration change of the analysed plasma (figure 1), it was surprising that a relatively small change of the inner SP position relative to the distance to the upper inner divertor region could produce such an increased surface heating where the D emission is observed. Also, the modification of the ELM characteristics when changing the configuration cannot explain the increased heat load. Neither the ELM frequency

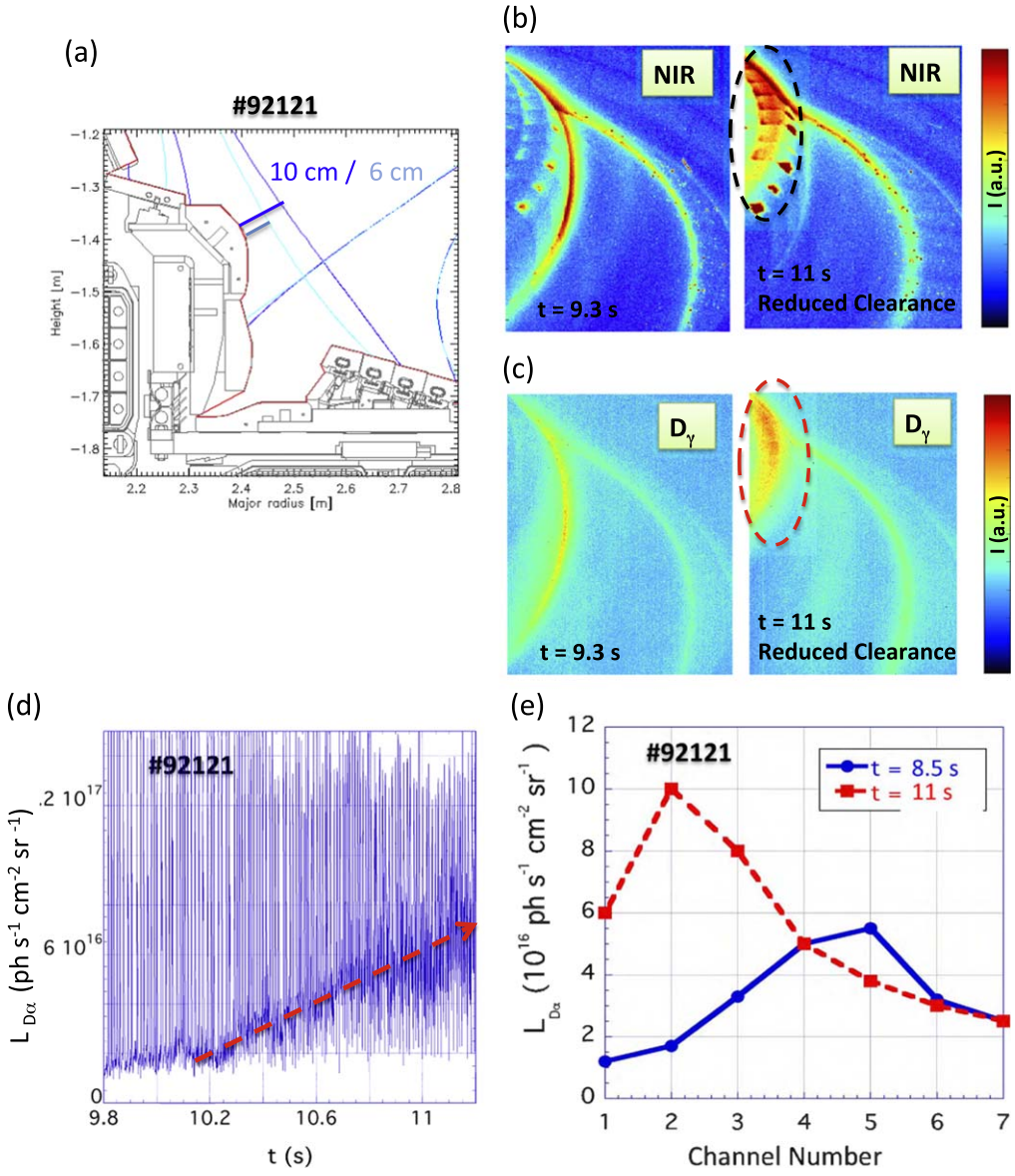

Figure 7. (a) Divertor configuration of #92121. (b) Two averaged images of the NIR camera and (c) D_γ-filtered camera. The left and right images correspond respectively to the larger and shorter clearance phases. (d) Time evolution of the innermost divertor Spectroscopy D_α-emission chord looking at tiles 0 and 1. (e) D_α-radiance profiles as a function of channel number and major radius R.

nor the ELM energy-loss (depicted from the pedestal T_e and n_e decays as well from the WI emission peak intensities) varied significantly with the configuration change. The only possible reason found for this temperature raise is following: when turning to V-configuration, the clearance (or gap) to the upper inner divertor corner at tile 1, defined as the distance from the material surface to the separatrix, was significantly reduced due to a change of the outer SP position. This can be seen in figure 1, where the respective clearances are marked with a blue arrow for the V-configuration (about 6 cm) and a red one for the C-configuration (about 12 cm). Assuming a typical SOL power decay length $\lambda_q = 3$ mm for high-power H-mode plasmas in JET at the outer midplane and taking into account the magnetic flux expansion at the inner divertor corner we determine that the heat flux becomes amplified there by a factor of about 30 in the V-configuration with the reduced clearance. Additionally, it is well-known that co-deposits reach much higher temperatures compared to the bulk material on which they are deposited due to their low thermal conductivity [43–46]. In fact, they appear as glowing 'Hot Spots' and can be distinguished quite easily from the bulk material even with visible cameras.

4. Other examples

To confirm the link between clearance at the upper inner divertor with the increased surface heating and the enhanced D_α-emission there, other plasmas have been analysed. Figure 7(a) shows the divertor configuration of #92121, where the position of the outer SP was changed along the outer horizontal target during the H-mode phase. Note that in

this case the inner SP was still placed on the vertical tile 3. While doing this, the clearance to the corner of tile 1 was reduced from approximately 10 to 6 cm. The gas puffing rate and the NBI power ($P = 14$ MW) was kept constant. Here the only significant global plasma variation after the configuration change to a reduced clearance was a 10% increase in plasma density and also a rise in the ELM frequency from 60 to 80 Hz. Concerning the thermal and D visible emission changes we see the following: figure 7(b) shows two images that are an average of ten frames corresponding to about 180 ms from the NIR Protection camera for the same discharge (again no MWIR camera available), left before and right after the clearance decrease. The increase of the thermal emission from hot spots clearly indicates an increased power load there when the clearance is reduced. Below in figure 7(c) are the images of a D_γ-filtered camera averaged over 200 ms with the same view (D_α was not available). Despite the unchanged inner SP position the emission distribution clearly changes; before the clearance reduction the dominant D emission at the inner divertor comes from the lower part of the vertical target near the inner SP position and after from the top of tile 1. Figure 7(d) shows the time evolution of the innermost divertor spectroscopy D_α-emission chord (channel number 1) looking on top of tiles 0 and 1. An increase of the base level (inter-ELM) during the clearance reduction by a factor of about 6 is observed. At the same time (not shown), the equivalent channels of BeII and WI raise just by a factor of 2, as does the ion saturation current of the innermost divertor LP on Tile 1 (see figure 1). This indicates that the clearance reduction induces in this region an increase of the ion flux by a factor of about 2 while that of the D_α-emission is three times larger. Since a significant increase of S/XB cannot be expected, this means that the neutral flux is strongly enhanced with respect to the incoming ion flux, which points again to local thermal desorption there. Figure 7(e) shows the clear displacement of the D_α-emission peak to the top of Tile 1 (channel number 2) during the inter-ELM period as obtained from the upper spectroscopy lines of sight in agreement with the D_γ-filtered camera (figure 7(c)).

Another similar example of clearance reduction without inner SP position change but where the MWIR thermography camera was available is shown in figure 8(a). The two equivalent discharges #83177 and #83491 had the following parameters: $B_T = 2.8$ T, $I_P = 2.5$ MA, $P = 16$ MW (NBI). They were already compared in another work to observe the effect when changing the outer SP from the horizontal to the vertical target [47]. The average images of the IR thermography video over 1 s (about 15 frames) of both plasmas during the H-mode of both discharges are shown to the right. For the plasma with reduced clearance the temperature at tiles 1 and 0 is in the range of about 300 °C–350 °C, much higher than the other one that just reaches about 200 °C. Figure 8(b) shows the inter-ELM D_α-emission distribution at the inner divertor (1 is innermost channel) for both discharges. The strong increase of the intensity for the reduced clearance plasma from tile 1 is again clearly visible.

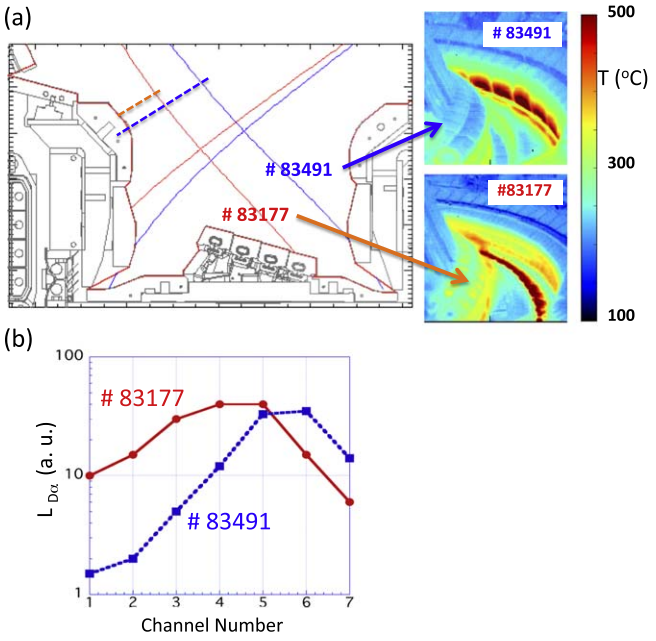

Figure 8. (a) Magnetic configurations of plasmas #83177 and # 83491 and to the right, two frames of each of the MWIR. (b) Inter-ELM D_α-radiance profiles at the inner divertor of both plasmas.

The last case study compares three plasmas with the following parameters: $B_T = 2.2$ T, $I_P = 2$ MA, $P = 13.5$ MW (NBI) + 1.5 MW (ICRF). As shown in figure 9(a), two of them had both SPs at the divertor but different puffing levels. In the third one the inner SP was moved to the vertical target. Note that the interesting point here is that the clearance to the upper inner divertor corner is not varied, only the inner SP position. These plasmas were already analysed to study the influence of divertor neutral pumping optimisation and gas injection rate on plasma edge properties and global plasma confinement at high triangularity [10]. The best confinement ($H_{98Y} \approx 1$) was achieved for the lowest puffing level (lowest pedestal density) and with both SPs at the divertor corners (#89341). Stable plasmas with the inner SP at the vertical target with such low gas injection rates could not be maintained due to the high tungsten influx. This was only possible in discharge #89340 when the gas level was at the same level as in #89334. In both plasmas the confinement degraded in about 20% independently of the divertor configuration. Their pedestal densities were similar, although the ELMs showed quite different characteristics [10], being much longer as in a quiescent H-mode for #89340. Making a similar analysis for this set of plasmas as done above we observe the following: The NIR camera showed that for increased puffing levels, at the inner divertor an increasingly strong volume emission evolves, which is an indication of the characteristic cool, high density, recombining SOL plasma, which happens to a similar degree in the C- (#89334) and the V-configuration (#89340). However, no 'Hot spots' are visible in either. The MWIR camera shows similar temperatures at tiles 0 and 1 for both configurations. Additionally, as shown in figure 9(b), the inter-ELM D_α-emission distribution at the inner divertor is

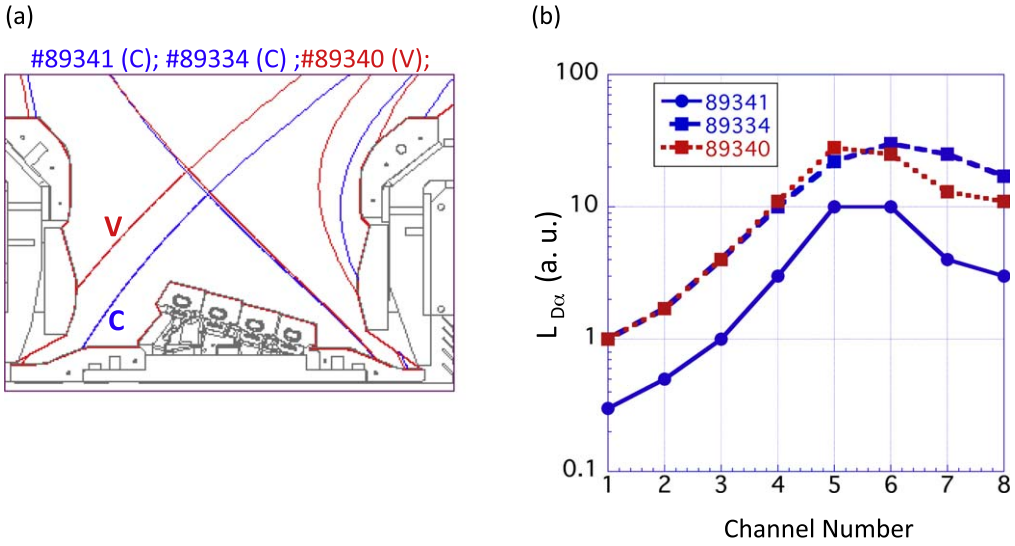

Figure 9. (a) Magnetic configurations of plasmas #89341, #89334 and #89340 and (b) inter-ELM D_α-radiance distribution in the inner divertor.

very similar for the three plasmas. The one with the lowest puffing is a factor of about 3 lower than the other two, which have similar intensities despite the different divertor configurations. There is no enhanced D_α-emission at the upper inner divertor for the plasma in the V-configuration here. Therefore it can be said that moving the inner SP position from the divertor corner a few centimetres up on the vertical target, without clearance modification, does not substantially modify the neutral flux distribution.

5. Using plasma configuration to induce fuel desorption from the upper inner divertor

It is well known that the Hydrogen isotope makeup of the plasma is not only composed of that injected by puffing to the plasma or by NBI, but also of the isotopes trapped in the reactor surface walls which re-enter the plasma during recycling. This is known as 'wall isotope exchange'. This process is used intentionally as a wall-conditioning technique to clean-up the reactor vessel. It has been already used in TFTR and JET to retrieve the trapped T from the walls after D–T experiments with repeated low power plasmas [48–51]. Separatrix scanning with high power plasmas has been also proposed elsewhere [52]. Wall isotope exchange has been also extensively studied using ICRF discharges with only toroidal magnetic fields to apply it to future superconducting reactors such as ITER [53–55]. A review on the different wall-conditioning techniques proposed for ITER can be found in [56].

More recently, dedicated experiments of isotope exchange in JET with the ILW using low-power L-mode plasmas showed a very weak access to the long-term retention reservoir in the co-deposited Be layers where most of the fuel becomes trapped [57]. Therefore alternative techniques to clean up the retained T in JET would be desirable. As already mentioned, it is known that fuel trapped in Be co-deposits in the divertor can be removed by heating the surface to temperatures >300 °C–350 °C [41, 42]. Unfortunately, such high temperatures can only be reached marginally by baking of the vacuum vessel in certain regions. Therefore, specific wall-conditioning techniques are proposed to prepare the next JET T campaigns with the ILW [58]. One of the proposed techniques is linked to the subject-matter of the present work, since the local outgassing from the Be co-deposits at the upper inner divertor is intentionally induced by plasmas with magnetic configurations that focus the ion and heat fluxes there. A preliminary analysis is shown in this section.

The discharge described here corresponds to a plasma from the beginning of a D campaign just after a H one. Figure 10(a) shows the magnetic configuration of the high-power plasma #91961 with $B_T = 3$ T, $I_P = 3.2$ MA and $P = 24$ MW (NBI). It was used to study W melting on tile 5 by directing the outer SP there. The inner SP was raised to the upper corner of tile 1 and the clearance there was quite small (6 cm). Figure 10(b) upper corresponds to a frame of the MWIR thermography camera during the NBI-phase and where two ROIs are defined corresponding to tiles 0 and 1. Below, the corresponding temperature evolutions are shown. The ROI corresponding to tile 1 surpasses the camera's saturation value with $T > 1100$ °C (note that half the value is shown) and the one of tile 0 reaches 600 °C. For these very high temperatures a strong outgassing at the upper inner divertor region must be expected.

Figure 11 shows the following time traces for this discharge: the NBI power P, the D puffing rate Q_0, the pressure measured in the lower sub-divertor duct p, the vertical coordinate of the inner SP Z_{SP} and the innermost D_α-radiance chord $L_{D\alpha,in}$. At the beginning Q_0 shows a pulse (marked with a circle and the number 1) to achieve the desired plasma density for the H-mode and later stays constant at a moderate value. The corresponding increase of the pressure p in this

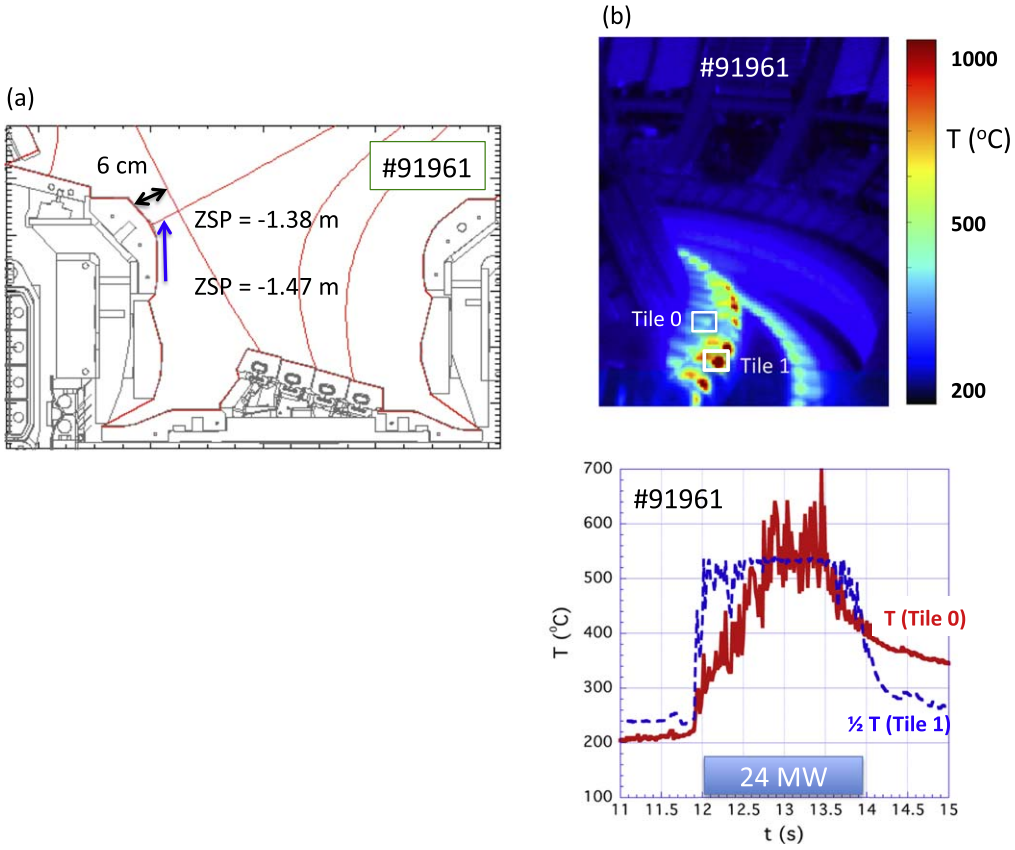

Figure 10. (a) Magnetic configuration of plasma #91961 and (b) frame of the MWIR thermography camera during the NBI-phase where two ROIs are defined corresponding to tiles 0 and 1 and, below, their corresponding temperature evolutions (note that the half value is shown for Tile 1).

puffing pulse is marked with a first red arrow. There is a time delay of p with respect to the Q_0 pulse due to the conductance of the tokamak vacuum vessel to the manometer location. The inner SP is raised at $t \geqslant 12$ s, when Z_{SP} increases (marked with a second circle and the number 2). Despite the constant puffing level, the neutral pressure shows a second increase with a similar time delay as before. Also at this moment, the surface temperatures of tiles 0 and 1 rise sharply (figure 10(b)). At the same time $L_{D\alpha,\,in}$ strongly increases and even saturates, which indicates a strong recycling/outgassing source at the upper inner divertor as we expected before.

The discharge analysed here was one of the first high power plasmas of a D campaign just after a long H campaign and one could expect that H isotopes had accumulated in the Be co-deposits of tiles 0 and 1. Therefore, if local heating and fuel outgassing was achieved by this D plasma, then some accumulated H isotope should have been desorbed. The lowest frame of figure 11 shows the time trace of the H isotope concentration (H/(H + D)) of the plasma as measured by an optical Penning gauge in the sub-divertor. There is a clear increase of this signal, that reached up to about 10% during the phase when tiles 0 and 1 were heated due to the inner SP raise. Note that before this, the H-concentration is $\leqslant$3%, which is below the detection limit. This is a clear indication that the plasma configuration with the raised inner SP was effective in desorbing trapped H at the upper inner Divertor region.

Future studies are planed before the next T campaign to try to confirm the potential use of this local plasma heating and outgassing effect at the upper inner divertor as a wall-conditioning technique for JET [58]. For the next T–T experiments, it is desired to remove all possible trapped D from the walls of previous campaigns, to minimise D–T fusion reactions. A H-campaign has been foreseen before the T one, to exchange as much as possible H by the previously trapped D. In this phase, the use of raised inner SP configurations to induce heating of tiles 0 and 1 will be studied in more detail. If useful, the same technique could be later applied to recover surface retained T at this region.

6. Discussion and summary

In the present work we have studied some aspects concerning the impact of the divertor configuration on recycling neutral fluxes for JET ILW high power H-mode plasmas. We analyse in detail the previously observed anomalously strong D_α-emission [24] that appears at the upper inner divertor for certain magnetic topologies just after the ELMs. For these plasmas, a systematic correlation has been found of this enhanced emission with a local surface temperature rise there. Since this region is where the thickest fuel-containing Be co-deposits accumulate, we believe that surface overheating of these are the origin of the outgassing. In fact, the measured

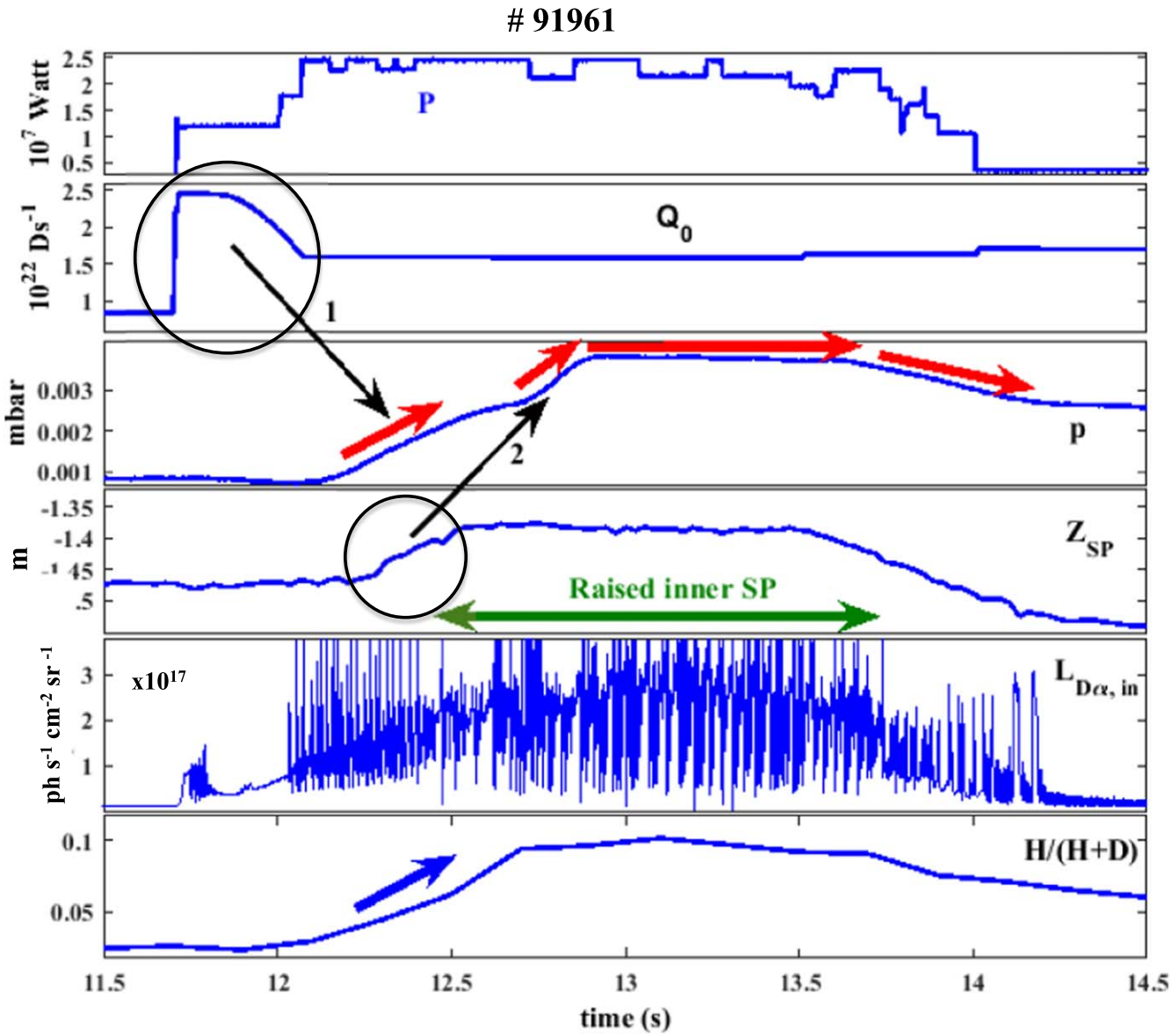

Figure 11. Time traces of plasma #91961: NBI power P, puffing flux Q_0, pressure measured in the sub-divertor duct p, the vertical coordinate of the inner SP Z_{SP}, the innermost D_α-radiance chord $L_{D\alpha,\ in}$ and Hydrogen concentration $H/(H + D)$.

surface temperatures locally exceed the typical thermal D release from these kinds of layers ($T > 350$ °C). The D emission happens just after the ELM-crash for a period of typically 5 ms. Its corresponding D neutral flux was quantified and dominates over puffing and the rest of recycling during this period of the ELM-cycle.

We propose that the origin of the local increased surface temperature for these plasma configurations is the increased heat flux due to the reduced distance from inner upper divertor corner to the separatrix (clearance). Additionally, it is well-known that co-deposits reach higher temperatures more easily compared to the bulk material on which they are deposited due to their low thermal conductivity. It must be acknowledged, however, that there is some uncertainty in the present absolute surface temperature measurements. This is because the co-deposits on top of the W-coated carbon tiles 0 and 1 probably alters the thermal surface emissivity, which is a parameter necessary to deduce the temperature. Future work is ongoing to experimentally measure the emissivity of these layers more accurately.

On the other hand, it should be noted that the clearance reduction at the upper inner divertor should, apart from locally increasing the heat flux there and possibly inducing fuel desorption, also have an important effect on the SOL-Edge plasma coupling. Decreasing the Separatrix distance from the material surface should facilitate the communication of the SOL in this region with the confined plasma edge. For example, the fuelling efficiency of the desorbed neutrals coming from this region, that may dominate after the ELM crash as shown here, most probably becomes enhanced, since their likelihood to cross the Separatrix before becoming ionised in the SOL increases with the reduced path (see

figure 1). Also the SOL radiation layer, usually dominant at the inner divertor close to the X-point, has a shorter distance to approach and even penetrate the Separatrix. This is something that potentially could produce a cooling of the plasma pedestal. Therefore we believe that, when analysing the effect of the divertor magnetic configuration on the plasma edge and pedestal properties, in addition to the SP proximity to the pumping openings or their position on vertical versus horizontal targets, the clearance at the upper inner divertor region should be also considered, at least when this is strongly reduced.

Finally, we have studied high-power ELMy H-mode plasmas with raised inner SP at the upper inner divertor corner to intentionally induce previously trapped D by thermal outgassing. By focussing the plasma ion and heat flux there, very high temperatures can be achieved well above the one needed to induce outgassing ($T > 1000$ °C) and as expected, strong D desorption from this region was observed. The preliminary analysis indicates that these plasmas can be used for wall isotope control and T recovery specifically in this reactor vessel region, complementarily to other wall-conditioning techniques [58]. More specific experiments are planned in the near future to continue this study and optimise the plasma parameters (power, magnetic shape, density, etc) for maximum conditioning efficiency.

Finally, we have studied high-power ELMy H-mode plasmas with raised inner SP at the upper inner divertor corner where most fuel-trapping beryllium co-deposits accumulate. By focussing the plasma ion and heat flux there, very high temperatures ($T > 1000$ °C) can be achieved, well above the one needed to induce outgassing. As expected, strong fuel emission from this region was observed. In fact, a H plasma was able to significantly desorb D gas, presumably trapped in the past in these long-term co-deposits. Therefore, the preliminary analysis indicates that these plasmas can be used for wall isotope control and T recovery specifically in this reactor vessel region, complementarily to other wall-conditioning techniques [58]. More specific experiments are planned in the near future to continue this study and optimise the plasma parameters (power, magnetic shape, density, etc) for maximum conditioning efficiency.

Acknowledgments

This work has been carried out within the framework of the EURO fusion Consortium and has received funding from the Euratom research and training programme 2014–2018 under grant agreement No. 633053. The views and opinions expressed herein do not necessarily reflect those of the European Commission.

Appendix

The use of equation (1) to estimate the D neutral flux F_0 through the D_α-radiance $L_{D\alpha}$ can be only used if the plasma is in ionising conditions, i.e. when recombination can be neglected. This has been checked to be the case here in two ways:

1. The ion flux of the uppermost LP (see figure 1) estimated from the ion saturation has a similar value (within a factor of two) to the neutral flux obtained locally from D_α-channel number 3, which observes an area very close to this probe. When the measured ion and neutral fluxes are similar, it means that recycling dominates over recombination.
2. It is known that in low temperature, high density recombining plasmas, the ratio of the Balmer lines D_γ/D_α increases from about 0.02 in ionising conditions to about 0.1 in recombining conditions [59]. This ratio was monitored using two visible-range spectrometers that collect the light of both atomic lines with the same lines of view as the fast D_α-Spectroscopy. Unfortunately their acquisition frequency is of about 40 Hz so that the signals are ELM-averaged. When looking at the Spectrometer channels that look at the upper inner divertor corner we obtain a ratio $D_\gamma/D_\alpha \approx 0.03$ during the whole H-mode phase (in C- and V- configuration), which is approximately the one expected in ionising conditions.

ORCID iDs

E de la Cal https://orcid.org/0000-0001-8020-7682
U Losada https://orcid.org/0000-0003-1161-8976
S Brezinsek https://orcid.org/0000-0002-7213-3326
A Huber https://orcid.org/0000-0002-3558-8129
F Militello https://orcid.org/0000-0002-8034-4756
S Wiesen https://orcid.org/0000-0002-3696-5475

References

[1] Brezinsek S *et al* 2013 *Nucl. Fusion* **53** 083023
[2] Matthews G F *et al* 2014 *Phys. Scr.* **T159** 014015
[3] F Romanelli on behalf of JET Contributors 2015 *Nucl. Fusion* **55** 104001
[4] Litaudon X *et al* 2017 *Nucl. Fusion* **57** 102001
[5] Giroud C *et al* 2013 *Nucl. Fusion* **53** 113025
[6] de la Luna E *et al* 2014 *25th IAEA FEC (Saint Petersburg, Russia)*
[7] Joffrin E *et al* 2014 *25th IAEA FEC (Saint Petersburg, Russia)*
[8] Solano E *et al* 2014 *Proc. 41st EPS Conf. on Plasma Physics (Berlin, Germany)*
[9] Tamain P *et al* 2015 *J. Nucl. Mater.* **463** 450
[10] de la Luna E *et al* 2016 *IAEA FEC*
[11] Joffrin E *et al* 2017 *Nucl. Fusion* **57** 086025
[12] Kaye S *et al* 1984 *J. Nucl. Mater.* **121** 115
[13] Horton L D *et al* 1999 *Nucl. Fusion* **39** 1
[14] Sengoku S *et al* 1987 *J. Nucl. Mater.* **145–147** 556
[15] Sengoku S *et al* 1989 *J. Nucl. Mater.* **162–164** 667
[16] Loarte A 2001 *Plasma Phys. Control. Fusion* **43** R183
[17] Kukushkin A S *et al* 2005 *Nucl. Fusion* **45** 608
[18] Brezinsek S *et al* 2015 *J. Nucl. Mater.* **463** 11
[19] Groth M *et al* 2013 *Nucl. Fusion* **53** 093016

[20] Järvinen A *et al* 2013 *Proc. 40th EPS Conf. on Plasma Physics (Espoo, Finland)*
[21] Wiesen S *et al* 2016 *Contrib. Plasma Phys.* **56** 754
[22] Harting D M *et al* 2015 *J. Nucl. Mater.* **463** 493
[23] Brenzisek S *et al* 2016 *Phys. Scr.* **T167** 014076
[24] Wiesen S *et al* 2017 *Nucl. Fusion* **57** 066024
[25] Guillemaut C *et al* 2018 *Nucl. Fusion* **58** 066006
[26] Marenkov E *et al* 2012 *Phys. Plasmas* **19** 092501
[27] Yu Pigarov A *et al* 2014 *Phys. Plasmas* **21** 062514
[28] de la Cal E and the TJ-II Team 2015 *Plasma Phys. Control. Fusion* **57** 075001
[29] Schmid K 2016 *Phys. Scr.* **T167** 014025
[30] Neverov V S *et al* 2019 *Nucl. Fusion* **59** 046011
[31] Horton L *et al* 2016 *Fusion Eng. Des.* **109–111** 925
[32] de la Cal E *et al* 2012 *Proc. 39th EPS Conf. on Plasma Physics (Stockholm, Sweden)*
[33] Huber A *et al* 2012 *Rev. Sci. Instrum.* **83** 10D511
[34] Gauthier E *et al* 2007 *Fusion Eng. Des.* **82** 1335
[35] Balboa I *et al* 2016 *Rev. Sci. Instrum.* **87** 11D419
[36] Arnoux G *et al* 2012 *Rev. Sci. Instrum.* **83** 10D727
[37] Huber A *et al* 2017 *Phys. Scr.* **T170** 014027
[38] Huber V *et al* 2017 *Fusion Eng. Des.* **123** 979
[39] Mayer M *et al* 2016 *Phys. Scr.* **T167** 014051
[40] Widdowson A *et al* 2017 *Nucl. Fusion* **57** 086045
[41] Alegre D *et al* 2017 *Phys. Scr.* **T170** 014028
[42] De Temmerman G *et al* 2017 *Nucl. Mater. Energy* **12** 267
[43] LaMarche P H *et al* 1986 *J. Vac. Sci. Technol.* A **4** 1198
[44] Gauthier E *et al* 2005 *J. Nucl. Mater.* **337–339** 960
[45] Gaspar J *et al* 2016 *Int. J. Thermal Sci.* **104** 292
[46] Mitteau R *et al* 2006 *Nucl. Fusion* **46** S49
[47] Leyland M J *et al* 2015 *Nucl. Fusion* **55** 013019
[48] Horton L D *et al* 1992 *J. Nucl. Mater.* **196–198** 139–42
[49] Andrew P *et al* 1992 *J. Nucl. Mater.* **196–198** 143
[50] Skinner C H *et al* 1997 *J. Nucl. Mater.* **241–243** 214
[51] Andrew P *et al* 1999 *Fusion Eng. Des.* **47** 233
[52] Higashijima S *et al* 1999 *J. Plasma Fusion Res.* **75** 1297 (in Japanese)
[53] de la Cal E and Gauthier E 1997 *Plasma Phys. Control. Fusion* **39** 1083
[54] Douai D *et al* 2011 *J. Nucl. Mater.* **415** S1021
[55] Wauters T *et al* 2011 *J. Nucl. Mater.* **415** S1033
[56] Shimada M *et al* 2011 *J. Nucl. Mater.* **415** S1013
[57] Loarer T *et al* 2015 *Nucl. Fusion* **55** 043021
[58] Borodkina I *et al* 2018 *Proc. 45th EPS Conf. on Plasma Physics O2.106 (Prague, 2018)*
[59] McCracken G M *et al* 1998 *Nucl. Fusion* **38** 619